J Polym Environ
DOI 10.1007/s10924-017-1089-z

ORIGINAL PAPER

Nanocomposites of Waterborne Polyurethane Reinforced with Cellulose Nanocrystals from Sisal Fibres

G. Mondragon[1] · A. Santamaria-Echart[1] · M. E. V. Hormaiztegui[2] · A. Arbelaiz[1] · C. Peña-Rodriguez[1] · V. Mucci[2] · M. Corcuera[1] · M. I. Aranguren[2] · A. Eceiza[1]

Abstract Cellulose nanocrystals (CNC) were isolated from sisal fibres and were incorporated in the form of an aqueous suspension to a waterborne polyurethane (WBPU) synthesized from components derived from natural sources using an aliphatic diisocyanate. Transparent nanocomposite films with different CNC contents were prepared using a casting method. The morphology, thermal behaviour and mechanical properties of the nanocomposite films were characterized. Homogeneous distribution of CNC in the WBPU, even at high CNC contents was observed, resulting in an increase of 100% in modulus for systems with 5 and 10 wt% of CNC, with high elongations around 650%.

Keywords Sisal fibres · Castor oil · Cellulose nanocrystals · Waterborne polyurethanes · Nanocomposite

Introduction

Environmental problems and public concern about climate change are promoting the use of renewable raw materials derived from animals or plants. Environmentally friendly polymeric materials have been gaining a great attention for their use in different research fields in order to replace petroleum-based polymers [1–5]. As examples, vegetable oils and lignocellulosic materials which are abundant, recyclable, biodegradable and sustainable natural materials, can be used to synthesize bio-based polymers and composites [1, 3, 5]. Moreover, with the aim to reduce emissions of organic volatile compounds, the research in waterborne systems has been boosted [6]. Thereby, waterborne polyurethanes (WBPU) have gained attention due to the ability to assemble in stable particles in water dispersions by the addition of covalently bonded internal emulsifiers [6–8]. In general, WBPU can be considered as block copolymers composed of alternating rich urethane segments, denoted as hard segment (HS), and polyol segments, denoted as soft segment (SS) [7, 9]. Their applicability is due to their unique properties such as high strength and high elongation at break, which can be modified by a variety of choices of starting monomers, catalysts, and reaction conditions [6–8]. Among the different applications of polyurethane dispersions, elastomers [10, 11], floor coverings and chemical resistant coatings [12–16], polymeric dyes [17] and specialty adhesives [16, 18], can be distinguished.

Waterborne polyurethanes synthesized from biobased raw materials have become increasingly important [11, 12]. In particular, polyols derived from vegetable oils are materials that can be used to synthesize WBPU with high contents of carbon derived from low-cost renewable natural sources. Madbouly et al. [5] directly used castor oil, which offers the advantage of being a non-edible oil, for the synthesis of aqueous polyurethane dispersions. Lu and Larock [19] synthesized WBPU from a soybean oil-based macrodiol, Gaikwad et al. [20] used a vegetable oil obtained from karanja and cottonseed as natural resources to obtain eco-friendly polyurethane coatings and Chen et al. [21]

✉ A. Eceiza
arantxa.eceiza@ehu.eus

[1] 'Materials + Technologies' Group, Chemical & Environmental Engineering Dep., Engineering College of Gipuzkoa, University of the Basque Country UPV/EHU, Pza. Europa 1., 20018 Donostia-San Sebastián, Spain

[2] 'Ecomaterials' Division, Instituto de Investigaciones en Ciencia y Tecnología de Materiales (INTEMA), Universidad Nacional de Mar del Plata (UNMdP) - Consejo Nacional de Investigaciones Científicas y Técnicas (CONICET), Av. Juan B. Justo 4302., 7600 Mar del Plata, Argentina

Published online: 28 July 2017

incorporated a linseed-oil based polyhydroxy fatty acids as ionic segments into WBPU dispersions.

Many types of diisocyanates are available like aliphatic 1,6-hexamethylene diisocyanate (HDI), cycloaliphatic isophorone diisocyanate (IPDI) and 4,4′-dicyclohexyl methane diisocyanate (HMDI) and aromatic diisocyanates such as 4,4′-diphenyl methane diisocyanate (MDI) and 2,4-toluene diisocyanate (TDI). Most of the reports on the production of WBPU have considered the use of cycloaliphatic diisocyanates, more specifically, IPDI. Aromatic diisocyanates are discarded against aliphatic or cyclic ones, since they can degrade into carcinogenic and mutagenic aromatic amines [22] which release toxic products, and react rapidly with the water during the dispersion step [6], making handling more difficult. For this reason, the interest on WBPU based on aliphatic diisocyanates like HDI is increasing [23, 24].

However, mechanical properties of many WBPU need to be improved to fulfill the requirements of some engineering applications. It has been shown that the addition of different forms of nanocellulose to PU matrices improved the physical and mechanical properties of the matrix [25–29] because cellulose nanocrystals (CNC) have a modulus near to that of a perfect crystal of native cellulose (~150 GPa) [30–32]. Cellulose is one of the most abundant polymers in the earth and it is the main natural polysaccharide and the main structural component of the plants [33]. Thus, it has become an interesting source of nanoreinforcements in the form of cellulose nanofibres (CNF) or CNCs, which are highlighted by their low density, high modulus and tensile strength, biodegradability, renewability and availability [31, 32].

Hence, the addition of CNC aqueous dispersions, as isolated by acid hydrolysis, to WBPU, is proposed as an effective and sustainable route from the environmental point of view for the preparation of nanocomposites [11, 34, 35]. This pathway ensures good compatibility with interactions between WBPU and CNC without chemical modification or surfactants, and also reduces the risk of irreversible agglomeration of CNC during drying, since the presence of the polymer prevents the free assembling during water removal. Generally, good compatibility between them is essential to enhance the final properties of the nanocomposites [25, 28]. In addition, bionanocomposites can be prepared by casting of WBPU/CNC mixtures, showing good film-forming ability at room temperature and high flexibility [28, 34–36].

The aim of this work is to develop bionanocomposite films based on a waterborne bio-based polyurethane matrix reinforced with different contents of CNC isolated from sisal fibres using a succession of specific chemical treatments as detailed in a previous work [2]. Firstly, a WBPU matrix was synthesized using components derived from renewable sources and HDI, which thereafter was mixed with an aqueous dispersion of CNC, being the mixture sonicated and subsequently casted in Teflon moulds for the preparation of the bionanocomposite films. The suspensions were characterized by dynamic light scattering (DLS), atomic force microscopy (AFM), Fourier transform infrared spectroscopy (FTIR). Additionally, the films were subjected to thermogravimetric analysis (TGA), differential scanning calorimetry (DSC), dynamic mechanical analysis (DMA) and mechanical tests.

Experimental

Materials

WBPU was synthesized using a macrodiol derived from castor oil (which would correspond to SS domains in phase separated systems) and 1,6-hexamethylene diisocyanate (HDI), kindly supplied by Bayer under the trade name Desmodur H, and 2,2-bis-(hydroxymethyl)-propionic acid (DMPA), provided by Aldrich (which would correspond to the HS in phase separated systems). Dibutyltin dilaurate (DBTDL) provided from Aldrich was used as catalyst and triethylamine (TEA), purchased from Aldrich, was employed to neutralize the ionic groups in the dispersion. Acetone was used to control the viscosity during the synthesis. The castor oil derived macrodiol was poly(2,2-dimethylpropylene sebacate) diol with 70% of carbon coming from renewable sources, determined by ASTM D 6866. The chemical structure was determined using H^1NMR spectroscopy [1]. The macrodiol hydroxyl number, determined using the standard procedure ASTM D 4274-05 test method A, was 80 mg KOH g^{-1}, leading to a molecular weight of 1320 g mol^{-1}. Prior to its use, the macrodiol was dried in a rotary evaporator under vacuum at 70 °C for 14 h. HDI, DMPA and acetone were used as received. However, TEA was dehydrated with Hydranal molecular sieve 0.3 nm (water adsorption capacity of 15%), supplied by Fluka, which had been previously dried at 55 °C under vacuum for 1 day.

Sisal fibres (S) used in this work were provided by Celulosa de Levante, S.A. from Spain. The reagents employed for the specific chemical treatments were sodium hydroxide pellets PA-ACS-ISO, glacial acetic acid QP, nitric acid PA-ISO (65% purity), sulphuric acid PA-ISO (96% purity), ethanol PA-ACS (96%, v/v purity) and toluene HPLC grade supplied by Panreac. All reagents were used as received without further purification.

Synthesis of WBPU

The polyurethane was synthesised by one step method. Thus, a castor oil derived macrodiol (18.0 g) was introduced into 250 mL four-necked round bottom flask equipped with mechanical stirrer and heated to 80 °C within a thermostatic bath until the diol completely melted and then, DMPA (1.14 g) was added while stirring to achieve the mixing of the reactants. After that, DBTDL (0.123 g) and HDI (4.46 g) were added dropwise, and the reaction was let proceeding at 80 °C for 3 h within the bath under a dry nitrogen atmosphere. The NCO/OH ratio was 1.2 and to reduce the viscosity of the prepolymer, 100 mL of acetone were poured into the flask. Then, the solution was cooled down to 60 °C and the carboxylic acid groups of DMPA were neutralized by the addition of TEA (0.83 g) during 30 min. Finally, the product was dispersed in 100 mL of deionized water under vigorous stirring. After stirring at room temperature overnight, the acetone was evaporated by rotary vacuum evaporation at 45 °C until the suspension volume was reduced to a WBPU solid content around 20 wt%. The pH of the resulting dispersion was 7.9.

CNC Preparation

The CNC were isolated from sisal fibres following a previously published protocol [2]. Briefly, the fibres were firstly subjected to a solvent mixture of ethanol/toluene (1:2 v/v) under reflux for about 6 h to remove the extractives (waxes and oils) and then, they were treated with 2 wt% NaOH solution for 12 h at 40 °C in order to swell the raw fibres. After this step, fibres were subjected to an alkali treatment with 7.5 wt% NaOH solution under reflux for 90 min to remove hemicelluloses and lignins. In order to extract sisal cellulose nanofibres (CNF), fibres previously washed until pH 6, were submitted to the acetylation treatment (HNO_3 + acetic acid) under reflux for 30 min and thereafter, these fibres were washed with deionized water to neutralize. Finally, sisal acetylated fibres were treated with 64 wt% sulphuric acid at 45 °C for 45 min under continuous stirring to isolate sisal CNC.

Preparation of Polyurethane-Cellulose Nanocomposites

In order to subject all the samples at the same drying time, films were prepared with a fixed total volume of 21 mL. 5 mL of WBPU were mixed with different volumes of CNC aqueous dispersions, and the water content was further adjusted in order to prepare the bionanocomposites. First, CNC water suspensions were strongly stirred around 12 h. Then, to prevent the aggregations and degradation of CNC, they were sonicated in ice bath for 30 min, followed by strongly stirring for 10 min with a WBPU fix volume (5 mL). Afterward, these mixtures were sonicated in ice bath for 30 min. Subsequently, the resulting suspension was cast in glass Petri dishes coated with Teflon paper and dried in an oven at 50 °C for 35–40 h depending on water content to obtain the nanocomposite films. Before characterization, the films were stored about 1 week at room temperature in a desiccator. The final nanocomposite films, containing 1, 3, 5 and 10 wt% CNC, were coded as WBPU1CNC, WBPU3CNC, WBPU5CNC and WBPU10CNC, respectively. As reference, a polyurethane film without nanocrystals was also prepared, named as WBPU.

Nanocomposites Characterization

Morphological Analysis

Atomic force microscopy was used in order to characterize isolated CNC and CNC dispersion in the nanocomposites. The samples were prepared by spin coating in both cases. Images were obtained at room temperature, in tapping mode, using an atomic force microscope (AFM) from Digital Instruments having a NanoScope III controller with a Multi Mode head (Veeco) with an integrated silicon tip/cantilever, applying a resonance frequency of about 180 kHz. The cantilever had a tip radius of 5–10 nm and was 125 μm long. Samples were prepared by pouring a drop of different suspensions on mica substrates rotating at a rate of 1200 rpm during 120 s.

DLS

Particle size of WBPU dispersions was analysed by DLS using a BI-200SM goniometer, from Brookhaven. The intensity of dispersed light was measured using a luminous source of He–Ne laser (Mini L-30, wavelength $\lambda = 637$ nm, 400 mW) and a detector (BI–APD) placed on a rotary arm which allows measuring the intensity at 90°. Samples were prepared mixing a small amount of aqueous dispersion with ultrapure water and measurements were carried out at 25 °C. Three measurements were performed for each dispersion.

FTIR

Attenuated total reflection Fourier transform infrared spectra were recorded on a Nicolet Nexus 670 FT-IR spectrometer equipped with a single horizontal Golden Gate ATR cell with ZnSe cell/crystal. All spectra were recorded within a range of 4000–750 cm^{-1} with a resolution of 8 $cm^{-1}$and accumulation of 64 scans.

TGA

Dynamic thermogravimetric measurements were performed by using a TGA/SDTA 851 Mettler Toledo instrument. Dynamic tests were run from 25 to 800 °C at a heating rate of 10 ºC/min. These tests were carried out under nitrogen atmosphere in order to prevent a thermoxidative degradation.

DSC Analysis

Differential scanning calorimetry experiments were carried out in a Mettler Toledo 822e equipment, provided with a robotic arm and with an electric intracooler as refrigerator unit. These analyses were performed for unfilled and filled samples to investigate the interactions between cellulosic nanocrystals and the matrix. WBPU and nanocomposite samples with a weight between 5 and 10 mg were sealed in aluminium pans and were heated from −75 to 180 °C at a scanning rate of 20 °C min^{-1} under a constant nitrogen flow. The inflection point of heat capacity change (ΔC_p) observed was considered as indicative of the glass transition temperature (T_g).The melting temperature (T_m) was taken as the temperature of the maximum of the endothermic peak, while the area under the peak was the corresponding melting enthalpy (ΔH_m). The relative crystallinity values (χ_c) for each nanocomposite was determined as previously reported [1] using Eq. (1):

$$\chi_c = \frac{\Delta H_m}{\omega \times \Delta H_{100}} \quad (1)$$

where ΔH_m is the experimental melting enthalpy value obtained by DSC and ΔH_{100} the heat of fusion of the crystalline phase in the neat polyurethane without CNC and determined by DSC, while ω is the weight fraction of polymeric material in the bionanocomposites.

DMA

DMA measurements were performed in tensile mode with an Eplexor 100 N analyser, Gabo equipment. Measurements were carried out at a scanning rate of 2 °C min^{-1} from −100 to 100 °C, using a static strain of 0.05%. The operating frequency was 1 Hz. The approximate dimensions of the films were $8 \times 2.5 \times 0.4$ mm^3.

Mechanical Tests

Tensile tests were carried out in a MTS Insight Tester with a 250 N load cell and pneumatic grips to hold samples, using Testwork 4.0 software to determine mechanical results. The mechanical properties [stress at yield (σ_y), tensile modulus (E_t), stress at break (σ_b) and strain at break (ε_b)] of the samples were determined from stress–strain curves obtained at a crosshead speed of 50 mm min^{-1}. Samples were cut (8 mm in length, 2.5 mm in width and 0.4 mm in thickness) and the average values of at least five samples for each system were reported. Their thickness was measured at three random positions using a micrometre.

Scanning Electron Microscopy

SEM was used to analyse the fracture surfaces of neat polymer and nanocomposites based on CNC fibers. SEM micrographs were performed by JSM-6400 (JEOL) equipment with a wolframiun filament operating at an accelerated voltage of 20 kV. All samples were coated with chromium using a Quorum Q150 TES metallizer.

Results and Discussion

Morphology of CNC and WBPU/CNC Nanocomposites Structure

The particle size distribution is a key parameter to evaluate WBPU dispersions stability. The particle size of the synthesized WBPU dispersion, determined by DLS, was 121.5 ± 25.0 nm, leading to visually stable dispersion over 4 months (Fig. 1a). The hydrolysis protocol used for CNC isolation also leaded to a stable CNC suspension (Fig. 1b). AFM topography and height profile images in Fig. 1c show rod like nanocrystals. The average length and diameter of sisal CNC, determined by AFM height images and profiles assuming nanocrystals to be cylindrical in shape [37], were 224 ± 53 and 5 ± 2 nm, respectively, thus yielding an average aspect ratio (L/D) of the CNC around 45. These values are in agreement with data reported in literature for CNC obtained from similar sources [28, 38, 39]. Transparent bionanocomposite films were obtained as observed in Fig. 1d.

AFM phase contrast images have been used as a measure of the CNC distribution in polyurethane matrix. Figure 2 shows the microstructure of the upper surface of spin coated samples of WBPU matrix and nanocomposites containing 1, 3, 5 and 10 wt% CNC. The lack of CNC large aggregates in the nanocomposites is taken as an indication of good dispersion of the CNC in polyurethane matrix.

Attenuated Total Reflection—FTIR

Infrared spectroscopy was used to identify the functional groups present in CNC, polymer matrix and their nanocomposites films. Figure 3 shows ATR-FTIR spectra of isolated CNC, macrodiol, WBPU and nanocomposites containing 3

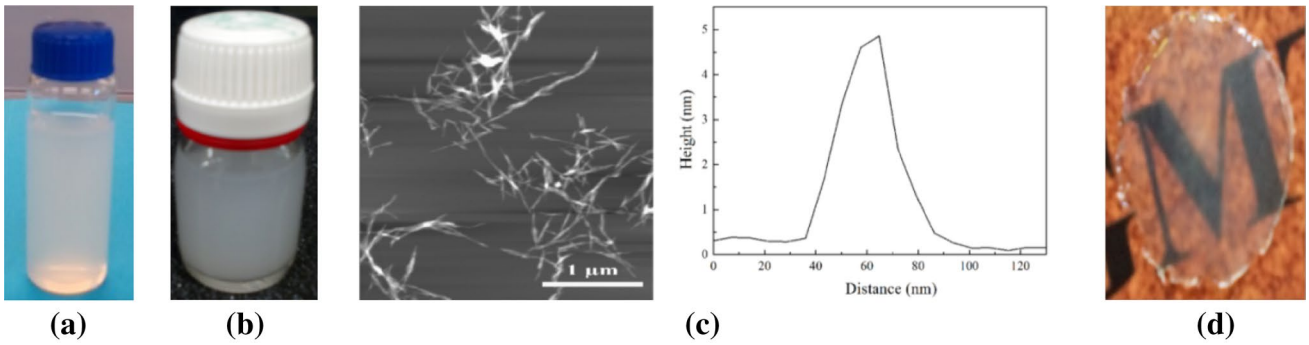

Fig. 1 WBPU (**a**) and CNC (**b**) suspensions and AFM of hydrolysed sisal CNC with their height profile CNC (**c**) and the transparency of WBPU5CNC nanocomposite film (**d**)

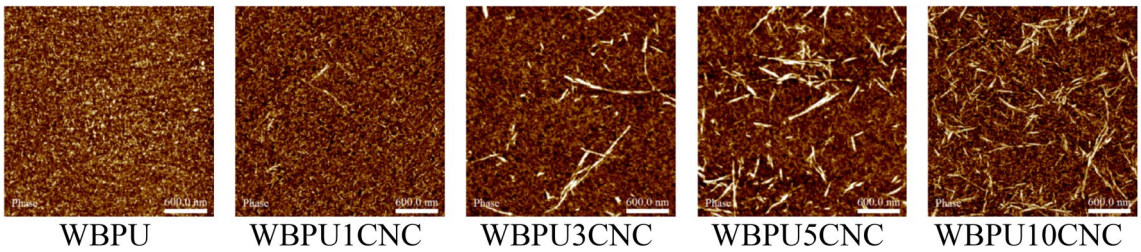

Fig. 2 AFM phase images of WBPU matrix and bionanocomposites with different CNC contents (*scale bar* 600 nm)

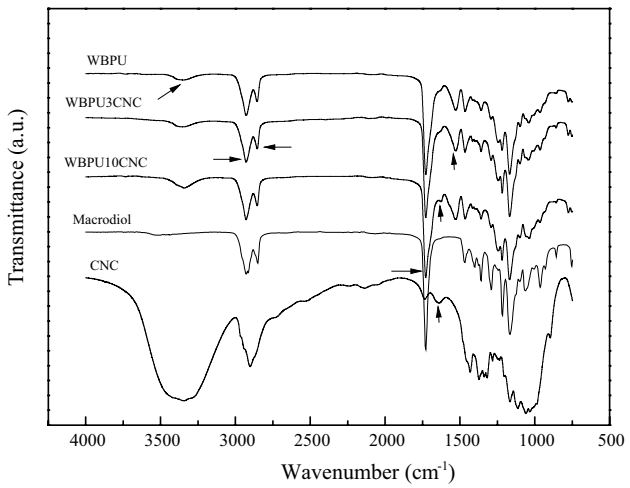

Fig. 3 FTIR spectra of macrodiol derived from castor oil, WBPU, CNC and bionanocomposites containing 3 and 10 wt% of CNC

and 10 wt% CNC. Primarily, as seen in neat WBPU and their nanocomposites spectra, the absence of the stretching vibration band at 2270 cm^{-1}, evidenced that WBPU synthesis reaction proceeded completely [1, 9]. The broad band observed between 3500–3000 cm^{-1} in CNC is related to the stretching vibration of O–H group. The band localized around 3348 cm^{-1} in WBPU sample, assigned to the N-H stretching vibration of urethane groups (υ_{-NH}) [1, 9, 35], becomes more pronounced in nanocomposite samples, due to overlapping with O–H stretching vibrations introduced by CNC [34–36]. The peaks located at 2927 and 2854 cm^{-1} correspond to the alkane C–H asymmetric and symmetric stretching vibrations [23]. Simultaneously, in the carbonyl stretching region (1800–1600 cm^{-1}) spectra of neat matrix and their nanocomposites, a band appears, which is attributed to both urethane and ester carbonyl from the macrodiol [11, 23]. With the purpose of analyzing the interactions between the matrix and CNCs, carbonyl groups region was studied. Using a curve-fitting procedure, the peak about 1728 cm^{-1} was deconvoluted in two Gaussian bands, which are associated to the free and hydrogen bonded C=O groups centered about 1730 and 1705 cm^{-1}, respectively. The ratio of the areas under the fitting curves corresponding to the hydrogen bonded and free C=O groups (A_{HB}/A_F), is related to the fraction of carbonyl groups involved in hydrogen bonding interactions. In this way, the effect of CNC incorporation to the hydrogen bonding formation in the nanocomposites was analyzed. Figure 4a shows a representative curve fitting for sample WBPU10CNC, and the values obtained from curves are summarized in Fig. 4b. It was observed that nanocomposites showed a higher A_{HB}/A_F ratio in comparison with the matrix (10–20% larger ratio than the one calculated for the matrix). This fact is related to the increase of C=O groups involved in hydrogen bonds, either with other C=O groups from the matrix

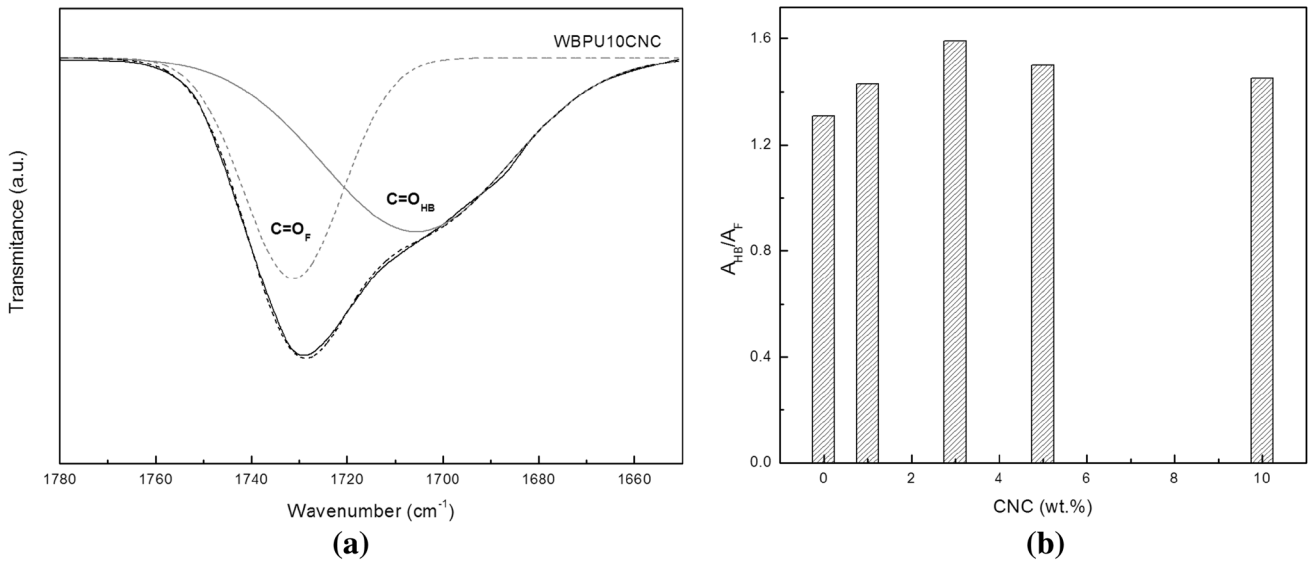

Fig. 4 Deconvolution of the carbonyl band in WBPU10CNC (**a**) and evolution of the ratio between free and bonded carbonyl groups area, A_{HB}/A_F with the CNC content (**b**)

or with OH groups of the CNC reinforcement. The A_{HB}/A_F ratio increased with the CNC concentration up to 3 wt% of CNC and decreased progressively at higher contents, suggesting that the increase of CNC content hindered effective WBPU-CNC interactions, probably due to CNC agglomerations. Further, the band at 1628 cm^{-1} observed in CNC and WBPU10CNC spectra could be related to absorbed water molecules in cellulose [2, 40, 41]. Moreover, as seen in neat WBPU and their nanocomposites spectra, a new band at 1527 cm^{-1} related to C–N stretching combined with N–H bending of urethane functional group, in amide II region, can be observed [9]. Additionally, the bands localized around 1038 and 1033 cm^{-1} in CNC spectrum are assigned to the C-O stretching vibration of the skeletal pyranose ring of cellulose [2, 41].

Thermal Analysis

TGA

Thermogravimetric analysis results allowed studying the thermal stability of the neat matrix and their bionanocomposites with different cellulose nanocrystal content. TGA and DTG thermograms for the neat matrix and the

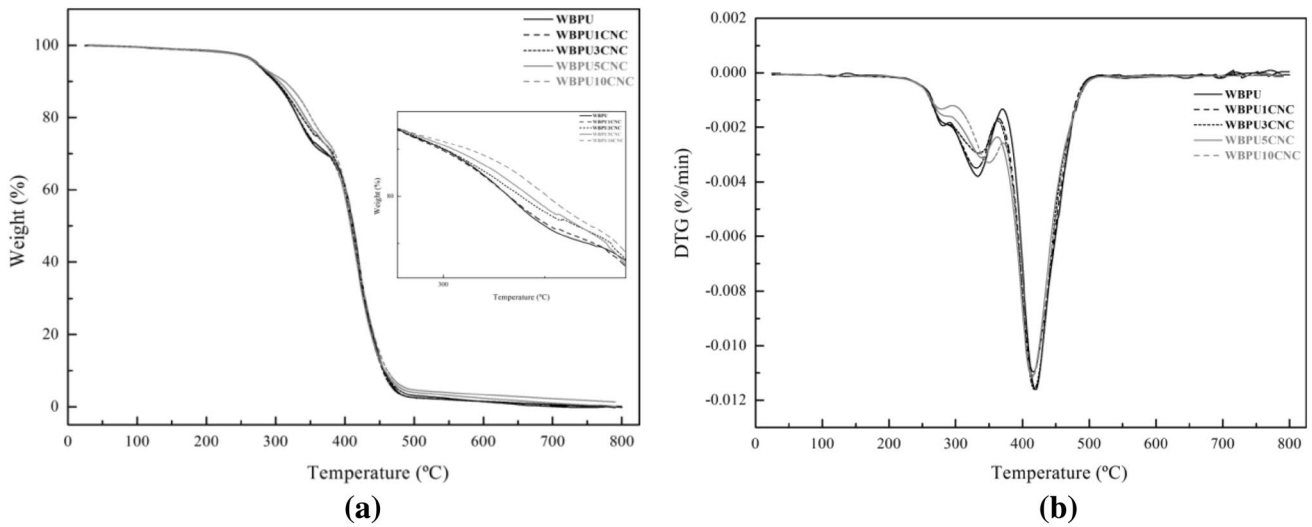

Fig. 5 TG (**a**) and DTG (**b**) curves obtained for neat polyurethane and their nanocomposites

bionanocomposites in nitrogen atmosphere are shown in Fig. 5. The thermal decomposition of the polyurethanes is given through several degradation steps due to different components that constitute their chemical structure [42, 43]. For WBPU matrix and bionanocomposites, two degradation steps can be distinguished. The first one, in the temperature range of 198–370 °C, corresponds to urethane bond degradation. The second one is related to the macrodiol rich domain and depends on its structure and three dimensional arrangements. It is clear that the thermal stability of WBPU matrix was improved as CNC weight content in the bionanocomposites was increased. This reduction in the rate of the first degradation stage in bionanocomposites compared with the corresponding one in the matrix is attributable to the stabilization of urethane groups by interactions with CNC (inset Fig. 5a) [43]. Additionally, the amount of residue of bionanocomposites at 800 °C slightly increased when nanocrystal content augmented. This could be due to the sulphate groups incorporated during the acid hydrolysis process of CNC isolation [2].

DSC

DSC first heating scan for the neat WBPU and nanocomposites are shown in Fig. 6a. Melting temperature (T_m), melting enthalpy (ΔHm), glass transition temperature (T_g) and the relative crystallinity (χ_{cSS}) of the polymer due to crystallization of the macrodiol moieties are reported in Table 1. At low temperatures, the scans of the WBPU and bionanocomposites showed a change in slope, which can be attributed to the glass transition temperature of the macrodiol rich domains (T_{gSS}). WBPU and all bionanocomposites showed similar T_{gSS} values, being higher than the value previously reported for neat macrodiol [1] (Fig. 6b). This indicates that there are few interactions between CNC and the amorphous regions of the WBPU [1, 44]. Similar results were found in the literature for bionanocomposites prepared from WBPU based

Table 1 Thermal properties of macrodiol, neat polyurethane and their nanocomposites

Sample	T_{gSS} (ºC)	T_{mSS} (ºC)	ΔH_{mSS} (Jg^{-1})[b]	χ_{cSS}[c]
Macrodiol	−60[a]	35, 58	112.0	–
WBPU	−44	37, 53	59.7	1
WBPU1CNC	−46	33, 50	55.1	0.93
WBPU3CNC	−45	31, 49, 61	57.3	0.99
WBPU5CNC	−46	30, 49, 61	63.1	1.11
WBPU10CNC	−45	31, 49, 59	54.7	1.02

[a][1]

[b]Calculated respect to total polyurethane weight

[c]Calculated with respect to the crystalline phase of the neat (unfilled) WBPU

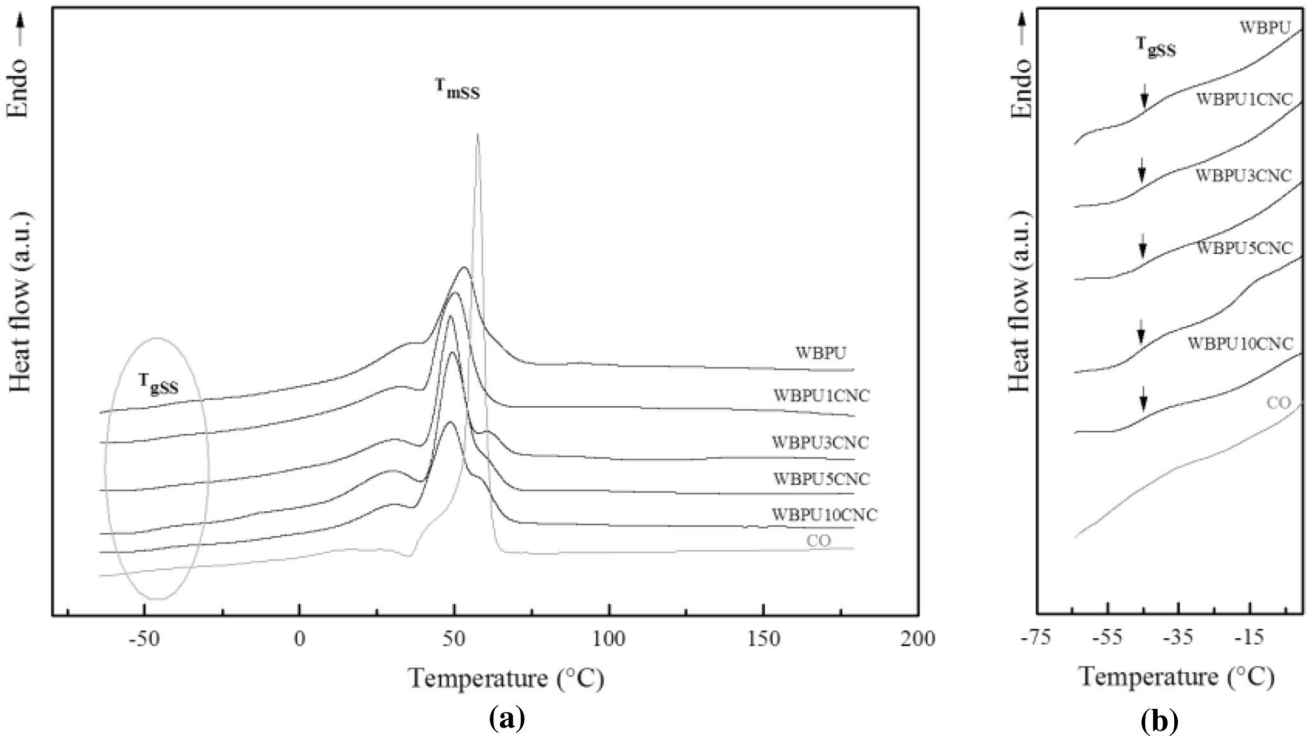

Fig. 6 DSC thermograms of first scan (**a**) and magnification of the low temperature range (**b**) of neat polyurethane and their nanocomposites

on a fossil sourced macrodiol and IPDI with different CNC contents, where the addition of CNC did not produce noticeable shifts in T_g values [25, 28, 34]. Regarding melting transition, a main peak with a shoulder at lower temperature can be observed for the neat macrodiol. The same peaks were observed for WBPU. However, in addition to the peaks observed for the WBPU, bionanocomposites showed a shoulder at higher temperature which became more noticeable at higher CNC content. These peaks can be related to different crystal structures. Moreover, the melting enthalpy, ΔH_{mSS}, decreases with addition of the minimum concentration of CNC used in this work. This is explained by the presence of CNC interfering with the mobility of the chains that would form the ordered crystalline phase. Thus, less perfect crystals (lower T_m) and lower melting enthalpy are reported. ΔH_{mSS} and related χ_{cSS} values suffer a slight increase when larger concentrations of CNC are used. This change with respect to the previous observation is related to a larger effect of the interactions between CNC and the WBPU [45] (as it was already discussed from the FTIR results on H-bonded urethanes). In the case of the DSC results, a new melting peak appears around 60 °C, corresponding to a different arrangement/ordering in the crystals and contributing to the total heat of melting. Since at high CNC concentrations, agglomeration is almost surely taking place, a new drop in the effect of CNC on crystallization can be observed, as it also was commented on the contribution of H-bonded carbonyl groups to the FTIR spectra.

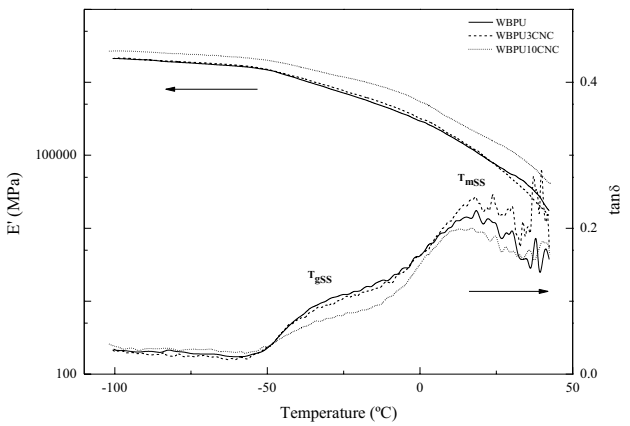

Fig. 7 Storage modulus and tan δ versus temperature of neat polyurethane and their nanocomposites

DMA

Dynamic mechanical analysis was performed on neat WBPU and bionanocomposites with different contents of CNC. Figure 7 shows the storage modulus (E′) and tan δ of WBPU, WBPU3CNC and WBPU10CNC samples. At temperatures below −50 °C, the E′ remains almost constant. Above this temperature, a drop in E′ value is observed associated to the glass transition of soft segments, which is reflected in a peak in tan δ curves. The relatively small drop of E′ at the transition and the wide range of temperature in which it occurs, suggests that phase separation (SS and HS) has essentially not taken place, which is the expected results from the one step synthesis of the WBPU [46]. Analyzing tan δ curves, similar glass transition values were observed in all samples in agreement with previous DSC results. Besides, the temperature range for this event (~−50 °C) agrees quite well with the location of T_{gSS} determined from DSC. Regarding the tan δ intensity in this region, a decrease is observed as CNC content increases, which can be due to the decrease in the content of the phase responsible for this transition and also to the restricted chain mobility resulting from polyurethane interactions with CNC [26–28]. As temperature increases above room temperature, a progressive decrease of E′ is seen, related to the broad interval of melting enthalpy as previously observed by DSC. Once crystals melting begins, the films start to flow. Comparing bionanocomposites and WBPU matrix, an increase in storage modulus (E′) is observed in WBPU10CNC sample, attributed to the well-dispersed nanocellulose and the effective reinforcing effect of CNC in the bionanocomposite [27, 34, 45, 47].

Tensile Testing Mechanical Results (MTS)

Mechanical properties of synthesized WBPU and their nanocomposites with different contents of CNC were

Table 2 Mechanical properties of neat polyurethane and their nanocomposites

Sample	Stress at yield, σ_y (MPa)	Modulus, E (MPa)	Stress at break, σ_b (MPa)	Strain at break, ε_b (%)
WBPU	3.23 ± 0.08	16.97 ± 1.00	11.66 ± 0.88	1425.49 ± 169.08
WBPU1CNC	3.05 ± 0.17	17.66 ± 0.82	8.76 ± 0.55	1161.26 ± 68.74
WBPU3CNC	3.00 ± 0.46	18.26 ± 1.75	9.58 ± 1.07	1161.48 ± 167.70
WBPU5CNC	4.37 ± 0.23	34.64 ± 2.23	7.21 ± 0.90	648.54 ± 117.22
WBPU10CNC	4.40 ± 0.17	35.09 ± 2.65	7.66 ± 0.49	712.44 ± 107.30

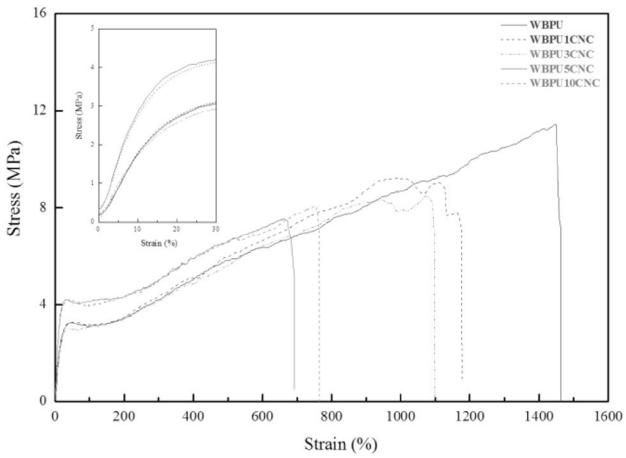

Fig. 8 Stress–strain curves of neat polyurethane and their nanocomposites. *Inset* stress–strain behavior in the low deformations interval

evaluated by tensile testing at room temperature. The different mechanical properties are summarized in Table 2.

As seen in Table 2, as CNC content increases, tensile modulus (E) values of WBPU bionanocomposites were significantly improved in comparison with those corresponding to the neat polyurethane. The bionanocomposites films showed an increase from 17 to 35 MPa, which is around 100% in WBPU5CNC and WBPU10CNC samples compared to the neat solid WBPU. The enhancement in stress at yield (σ_y) values observed at high CNC contents is directly attributable to CNC addition to matrix owing to the high stiffness and their reinforcing effect and probably, to the H-bonding between cellulose and PU and to the new crystals observed by DSC [26, 45, 47–49]. On the other hand, as depicted in Fig. 8 and summarized in Table 2, both stress (σ_b) and strain at break (ε_b) values are decreased in all nanocomposites respect to neat matrix. This decrease was associated to the CNC-polymer interactions that affect the crystal nucleation effect of the soft segments of the WBPU and to the intrinsic rigidity of the cellulose that restricts the mobility of the polymer chains [45, 47–49]. However, although the strain at break (ε_b) values decreased, bionanocomposites still maintained high deformations. A decrease in stress at break (σ_b) from 11.66 to 7.66 MPa with increasing filler content from 0 to 10 wt% was observed, related to the loss in ductility. Moreover, the percolation threshold in the nanocomposite was estimated theoretically as previously reported in the literature [35] and the calculated value was 2.3 wt%. However, the mechanical properties data suggested that the percolation threshold value was higher than 3 wt%. The difference between the percolation threshold values estimated and experimentally observed could be related, probably, to the high dispersion of length and diameter of the CNC. Cao et al. [35] observed that at

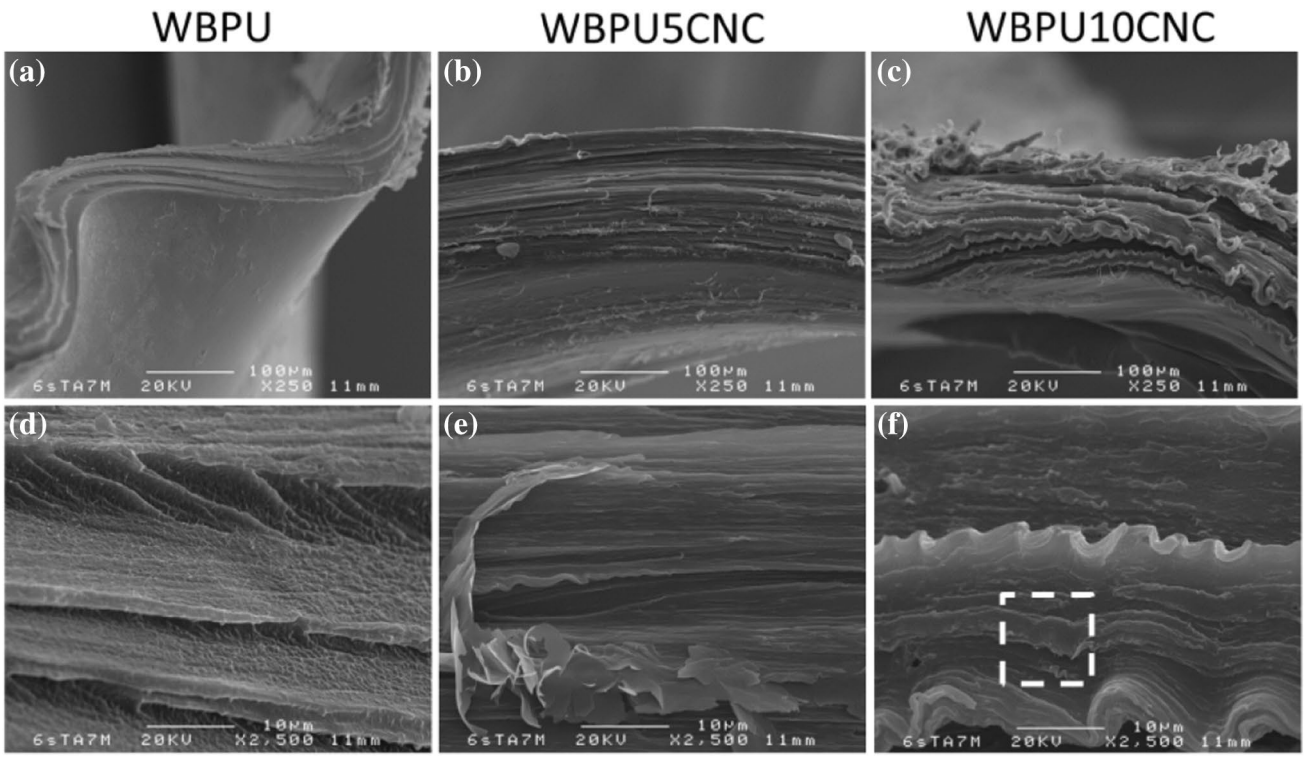

Fig. 9 SEM micrographs of tensile fracture surface of WBPU (**a, d**), WBPU5CNC (**b, e**) and WBPU10CNC nanocomposite (**c, f**) taken at different magnifications

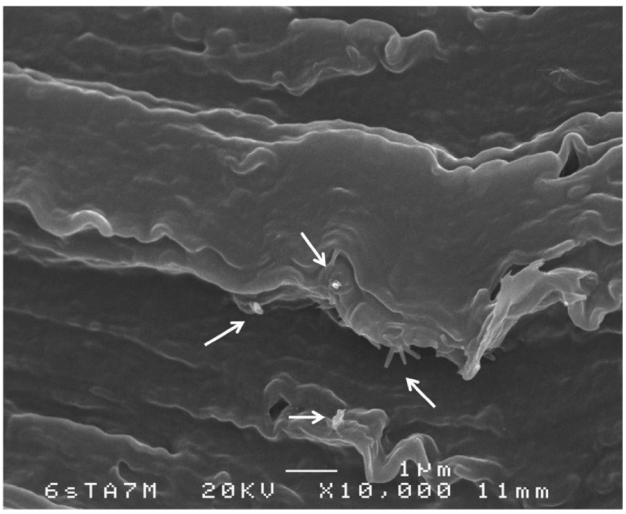

Fig. 10 SEM magnification of the area delimited by the *dashed square* taken from Fig. 9f (*arrows* denote CNCs)

CNC loading higher than percolation threshold value, the deformation at break decreased considerably, and this is the trend observed in our work. Below percolation, there is little effect of adding CNC, an observation that has been reported in the literature. On the contrary, at the highest CNC concentrations used in this work a percolated cellulose network is expected to be formed, which would reduce the ultimate deformation of the nanocomposites. It would be best to use 5% of CNC (which is a concentration above the percolation threshold), to obtain improved properties.

The scanning electron microscope (SEM) images of the tensile fracture surfaces of the matrix and nanocomposites containing 5 and 10 wt% of CNC showed different feature (Fig. 9). At the lowest magnification, nanocomposites seems to have rougher fracture surface than the matrix, which increases with the content of CNC, however at higher magnification the surface of neat WBPU seem to show higher plastic deformation which is in agreement with mechanical results. Regarding compatibility between CNC and matrix, CNC hardly can be observed in SEM image (Fig. 10), suggesting that they are mainly coated by the polymer matrix. In the magnified SEM image some CNC can be observed.

Conclusions

CNC have been successfully isolated from CNF sisal fibres based on successive chemical treatments, leading to rod-like CNC, with high aspect ratio.

A bio-based WBPU has been synthesized using a one-step method and employed in the preparation of nanocomposites containing 1, 3, 5 and 10 wt% of CNC from sisal fibres. Transparent films up to 10 wt% content of CNC were prepared by casting showing an uniform appearance. As observed by FTIR, the effective interactions between CNC and WBPU affected the crystal nucleation of the soft segments as also observed by DSC. An increase of 100% in modulus was observed for WBPU5CNC and WBPU10CNC, but maintaining relatively high elongations around 650%. The observed improvements were related to the reinforcing effect of CNC and the effect on the crystallization (nucleation) of the soft segment domains.

Acknowledgements Financial support from the Basque Country Government in the frame of Grupos Consolidados (IT-776-13) and Elkartek Program (KK-2016/00043), from Spanish Ministry of Economy and Competitiveness (MINECO) (MAT2013-43076-R) and from European Union-FP7-PIRSES-GA-2012-BIOPURFIL program is gratefully acknowledged. G. Mondragon wishes to acknowledge the Basque Government for his PhD Grant (BFI-2010-210). Moreover, technical support provided by SGIker unit from the University of the Basque Country is also gratefully acknowledged. The Argentinian coauthors wish to acknowledge the support of the National Agency for the Promotion of Science and Technology of Argentina (Project PICT 2013-1535), the National Research Council of Argentina, CONICET (PIP 00866) and the Universidad Nacional de Mar del Plata (15/G430-ING436/15).

References

1. Saralegi A, Rueda L, Fernandez-d'Arlas B, Mondragon I, Eceiza A, Corcuera MA (2012) Thermoplastic polyurethanes from renewable resources: effect of soft segment chemical structure and molecular weight on morphology and final properties. Polym Int 62:106–115
2. Mondragon G, Fernandes S, Retegi A, Peña C, Algar I, Eceiza A, Arbelaiz A (2014) A common strategy to extracting cellulose nanoentities from different plants. Ind Crop Prod 55:140–148
3. Gogoi S, Karak N (2014) Biobased biodegradable waterborne hyperbranched polyurethane as an ecofriendly sustainable material. ACS Sustain Chem Eng 2:2730–2738
4. Mondragon G, Peña-Rodriguez C, González A, Eceiza A, Arbelaiz A (2015) Bionanocomposites based on gelatin matrix and nanocellulose. Eur Polym J 62:1–9
5. Madbouly SA, Xia Y, Kessler MR (2013) Rheological behavior of environmentally friendly castor oil-based waterborne polyurethane dispersions. ACS 46:4606–4616
6. Noble K-L (1997) Waterborne polyurethanes. Prog Org Coat 32:131–136
7. Nelson AM, Long TE (2014) Synthesis, properties, and applications of ion containing polyurethane segmented copolymers. Macromol Chem Phys 215:2161–2174
8. Jaudouin O, Robin JJ, Lopez-Cuesta JM, Perrin D, Imbert C (2012) Ionomer-based polyurethanes: a comparative study of properties and applications. Polym Int 61:495–510
9. Santamaria-Echart A, Arbelaiz A, Saralegi A, Fernández-d'Arlas B, Eceiza A, Corcuera MA (2015) Relationship between reagents molar ratio and dispersion stability and film properties of waterborne polyurethanes. Coll Surf A 482:554–561
10. Jiang X, Li J, Ding M, Tan H, Ling Q, Zhong Y, Fu Q (2007) Synthesis and degradation of nontoxic biodegradable waterborne

polyurethanes elastomer with poly(e-caprolactone) and poly(ethylene glycol) as soft segment. Eur Polym J 43:1838–1846
11. Gao Z, Peng J, Zhong T, Sun J, Wang X, Yue C (2012) Biocompatible elastomer of waterborne polyurethane based on castor oil and polyethylene glycol with cellulose nanocrystals. Carbohydr Polym 87:2068–2075
12. Remya VR, Patil D, Abitha VK, Rane AV, Mishra RK (2016) Biobased materials for polyurethane dispersions. Chem Int 2:158–167
13. Howarth GA (2003) Polyurethanes, polyurethane dispersions and polyureas: Past, present and future. Surf Coat Int Part B 86:111–118
14. Meng QB, Lee S-L, Nah C, Lee Y-S (2009) Preparation of waterborne polyurethanes using an amphiphilic diol for breathable waterproof textile coatings. Prog Org Coat 66:382–386
15. Pan H, Chen D (2009) Waterborne polyurethane coating and its new applications in plush finishing. Text Res J 79:687–693
16. Hu J, Peng K, Guo J, Shan D, Kim GB, Li Q, Gerhard E, Zhu L, Tu W, Lv W, Hickner MA, Yang J (2016) Click cross-linking-improved waterborne polymers for environment-friendly coatings and adhesives. ACS Appl Mater Interfaces. doi:10.1021/acsami.6b02131
17. Mao H, Wang Y, Yao D, Wang C, Sun S (2016) Synthesis of blocked waterborne polyurethane polymeric dyes with tailored molecular weight: thermal, rheological and printing properties. RSC Adv 6:56831–56838
18. Orgilés-Calpena E, Arán-Aís F, Torró-Palau AM, Orgilés-Barceló C, Martín-Martínez JM (2009) Effect of annealing on the properties of waterborne polyurethane adhesive containing urethane-based thickener. Int J Adhes Adhes 29:774–780
19. Lu Y, Larock RC (2008) Soybean-oil-based waterborne polyurethane dispersions: Effects of polyol functionality and hard segment content on properties. Biomacromolecules 9:3332–3340
20. Gaikwad MS, Gite VV, Mahulikar PP, Hundiwale DG, Yemul OS (2015) Eco-friendly polyurethane coatings from cottonseed and karanja oil. Prog Org Coat 86:164–172
21. Chen R, Zhang C, Kessler MR (2014) Anionic waterborne polyurethane dispersion from bio-based ionic segment. RSC Adv 4:35476–35483
22. Janik H, Marzec M (2015) A review: fabrication of porous polyurethane scaffolds. Mater Sci Eng C 48:586–591
23. Xie D-Y, Song F, Zhang M, Wang X-L, Wang Y-Z (2016) Roles of soft segment length in structure and property of soy protein isolate/waterborne polyurethane blend films. Ind Eng Chem Res 55:1229–1235
24. Wu H, Li Z, Bai L, Zhu L, Gu J (2015) Research on the blocking reaction kinetics and mechanism of aqueous polyurethane micelles blocked by 2,4,6-trichlorophenol. J Macromol Sci Part A 52:847–855
25. Auad ML, Contos VS, Nutt S, Aranguren MI, Marcovich NE (2008) Characterization of nanocellulose reinforced shape memory polyurethanes. Polym Int 57:651–659
26. Lin S, Huang J, Chang PR, Wei S, Xu Y, Zhang Q (2013) Structure and mechanical properties of new biomass-based nanocomposite: castor oil-based polyurethane reinforced with acetylated cellulose nanocrystal. Carbohydr Polym 95:91–99
27. Pei A, Malho J-M, Ruokolainen J, Zhou Q, Berglund LA (2011) Strong nanocomposite reinforcement effects in polyurethane elastomer with low volume fraction of cellulose nanocrystals. Macromolecules 44:4422–4427
28. Benhamou K, Kaddami H, Magnin A, Dufresne A, Ahmad A (2015) Bio-based polyurethane reinforced with cellulose nanofibers: a comprehensive investigation on the effect of interface. Carbohydr Polym 122:202–211
29. Li Y, Ragauskas AJ (2011) Cellulose nano whiskers as a reinforcing filler in polyurethanes In: Reddy B (ed) Advances in diverse industrial applications of nanocomposites, InTech, Rijeka. ISBN: 978-953-307-202-9
30. Vincent JFV (1999) From cellulose to cell. J Exp Biol 202:3263–3268
31. Eichhorn SJ, Dufresne A, Aranguren M, Marcovich NE, Capadona JR, Rowan SJ, Weder C, Thielemans W, Roman M, Renneckar S, Gindl W, Veigel S, Keckes J, Yano H, Abe K, Nogi M, Nakagaito AN, Mangalam A, Simonsen J, Benight AS, Bismarck A, Berglund LA, Peijs T (2010) Review: current international research into cellulose nanofibres and nanocomposites. J Mater Sci 45:1–33
32. Mariano M, El Kissi N, Dufresne A (2014) Cellulose nanocrystals and related nanocomposites: Review of some properties and challenges. J Polym Sci Part B 52:791–806
33. Klemm D, Heublein B, Fink HP, Bohn A (2005) Cellulose: fascinating biopolymer sustainable raw material. Angew Chem Int Ed 44:3358–3393
34. Santamaria-Echart A, Ugarte L, Arbelaiz A, Gabilondo N, Corcuera MA, Eceiza A (2016) Two different incorporation routes of cellulose nanocrystals in waterborne polyurethane nanocomposites. Eur Polym J 76:99–109
35. Cao X, Dong H, Li CM (2007) New nanocomposite materials reinforced with flax cellulose nanocrystals in waterborne polyurethane. Biomacromolecules 8:899–904
36. Santamaria-Echart A, Ugarte L, García-Astrain C, Arbelaiz A, Corcuera MA, Eceiza A (2016) Cellulose nanocrystals reinforced environmentally-friendly waterborne polyurethane nanocomposites. Carbohydr Polym 151:1203–1209
37. Kvien I, Tanem BS, Oksman K (2005) Characterization of cellulose whiskers and their nanocomposites by atomic force and electron microscopy. Biomacromolecules 6:3160–3165
38. Siqueira G, Bras J, Dufresne A (2009) Cellulose whiskers versus microfibrils: influence of the nature of the nanoparticle and its surface functionalization on the thermal and mechanical properties of nanocomposites. Biomacromolecules 10:425–432
39. de Rodriguez NLG, Thielemans W, Dufresne A (2006) Sisal cellulose whiskers reinforced polyvinyl acetate nanocomposites. Cellulose 13:261–270
40. Lojewska J, Miśkowiec P, Łojewski T, Proniewicz LM (2005) Cellulose oxidative and hydrolytic degradation: in situ FTIR approach. Polym Degrad Stab 88:512–520
41. Alemdar A, Sain M (2008) Isolation and characterization of nanofibres from agricultural residues – Wheat straw and soy hulls. Bioresour Technol 99:1664–1671
42. Corcuera MA, Rueda L, Saralegui A, Martın MD, Fernandez-d'Arlas B, Mondragon I, Eceiza A (2011) Effect of diisocyanate structure on the properties and microstructure of polyurethanes based on polyols derived from renewable resources. J Appl Polym Sci 122:3677–3685
43. Wik VM, Aranguren MI, Mosiewicki MA (2010) Castor oil-based polyurethanes containing cellulose nanocrystals. Polym Eng Sci 51:1389–1396
44. Rueda-Larraz L, Fernández d'Arlas B, Tercjak A, Ribes A, Mondragon I, Eceiza A (2009) Synthesis and microstructure-mechanical property relationships of segmented polyurethanes based on a PCL-PTHF-PCL block copolymer as soft segment. Eur Polym J 45:2096–2109
45. Saralegi A, Gonzalez ML, Valea A, Eceiza A, Corcuera MA (2014) The role of cellulose nanocrystals in the improvement of the shape-memory properties of castor oil-based segmented thermoplastic polyurethanes. Compos Sci Technol 92:27–33
46. Hormaiztegui MEV, Mucci VL, Santamaria-Echart A, Corcuera MA, Eceiza A, Aranguren MI (2016) Waterborne polyurethane nanocomposites based on vegetable oil and microfibrillated cellulose. J Appl Polym Sci 133:44207

47. Wu Q, Henriksson M, Liu X, Berglund LA (2007) A high strength nanocomposite based on microcrystalline cellulose and polyurethane. Biomacromolecules 8:3687–3692
48. Saralegi A, Rueda L, Martin L, Arbelaiz A, Eceiza A, Corcuera MA (2013) From elastomeric to rigid polyurethane/cellulose nanocrystal bionanocomposites. Compos Sci Technol 88:39–47
49. Marcovich NE, Auad ML, Bellesi NE, Nutt SR, Aranguren MI (2006) Cellulose micro/nanocrystals reinforced polyurethane. J Mater Res 21:870–881